Alexandria Engineering Journal (2018) 57, 2265–2277

Alexandria University

Alexandria Engineering Journal

www.elsevier.com/locate/aej
www.sciencedirect.com

ORIGINAL ARTICLE

# Flow characteristics in low-speed wind tunnel contractions: Simulation and testing

**E.-S. Zanoun** *

*Department of Aerodynamics and Fluid Mechanics, Brandenburg University of Technology, Siemens-Halske-Ring 14, D-03046 Cottbus, Germany*
*Mechanical Engineering Department, Faculty of Engineering, Benha University, Benha 13512, Egypt*

Received 18 October 2016; revised 7 May 2017; accepted 23 August 2017
Available online 18 September 2017

**KEYWORDS**

Wind tunnel;
Contraction;
Numerical simulations;
Experimental flows

**Abstract** A numerical and experimental study was conducted to characterize flow through low-speed wind tunnel contractions. The simulations were carried out using an incompressible, two-dimensional flow solver based on finite volume scheme, predicting flow along the core, and at immediate vicinity of the wall of three pre-selected wall-shape contractions. The numerical results have been validated against experimental data obtained, utilizing laser-Doppler anemometer (LDA). Particular attentions have been given to the bulk flow velocity, the centerline mean velocity, the centerline velocity fluctuations, the uniformity of the mean velocity distribution at contraction's exit, and to the mean pressure coefficient. The experimentally determined mean-pressure coefficient values along the centerline and at contraction exit were found to be similar to those predicted numerically. The fifth-order polynomial contraction showed, however, good flow characteristics at the exit plane with small non-uniformity when compared to both the two-cubic arcs and the Witoszynski second-order polynomial contractions. It was therefore adopted for the **Co**ttbus **La**rge **pipe** (**CoLaPipe**) facility at the Department of Aerodynamics and Fluid Mechanics (LAS), BTU-Cottbus-Sefftenberg.



## 1. Introduction

Contractions are encountered in variety of engineering applications, e.g., in firefighting, flow mixing, foam control, medical applications, jet engines [1], and testing of green energy wind turbines in wind tunnels [2]. Wind, water and oil tunnels represent, therefore, basic experimental tools in optimization of such engineering application through testing physical models and validating numerical simulations. An integral part in those experimental facilities is the contraction section located ahead of the tunnel test section. The contractions are usually to be used to accelerate the flow and reduce variations in both the mean and fluctuating velocities, resulting in uniform and steady stream velocity distribution at the inlet of the tunnel test section, see e.g. Abdelhamed et al. [3]. The contractions are also to be considered as flow rates measuring devices in tunnel facilities for calibrating the non-direct measuring techniques

* Address: Department of Aerodynamics and Fluid Mechanics, Brandenburg University of Technology, Siemens-Halske-Ring 14, D-03046 Cottbus, Germany.
E-mail address: el-sayed.zanoun@b-tu.de.

Peer review under responsibility of Faculty of Engineering, Alexandria University.

http://dx.doi.org/10.1016/j.aej.2017.08.024

such as hot-wire anemometry. Hence, characterizing flow utilizing either numerical or experimental techniques in contractions is extremely important for the provision of flow quality in those various applications. To achieve this, the so-called contraction ratio, contraction wall shape, and contraction length are to be pre-selected and then optimized. All these parameters determined are in fact affecting the extent of flow uniformity, boundary layer flow separation, as well as the downstream turbulence level at the contraction exit or inside the tunnel test section. Better understanding, therefore, for flow through the tunnel various components, in particular, the contraction section is of vital importance, motivating the present study.

Over decades, several papers have been appeared addressing issues regarding the selection of contraction ratio, and wall shape as well as measuring performance, [see e.g. [4–13]]. For instance, to have smooth flow free from separation within a contraction, a proper selection of the contraction ratio and wall shape is needed, resulting in the production of uniform and steady streams at the contraction exit plane, see e.g. Gupta et al. [14], and Abdelhamed et al. [3]. For most of the low-speed wind tunnels, a contraction ratio between 6 and 12 is recommended, see Bradshaw and Paukhurt [15], Hussain and Ramjee [7], and Bell and Mehta [16]. It was claimed that once the contraction ratio is specified, the contraction shape and length become the next important design parameters, see Bradshaw and Paukhurt [15], and Hussain and Ramjee [7]. The contraction length is, however, a critical design parameter, determining the boundary layer thickness at the contraction exit. A shorter contraction might be proposed that minimizes the boundary layer thickness at the contraction exit in addition to savings in space and cost. However, it was observed by Morel [5] that as the contraction length is getting shorter the risk of the boundary layer separation increases as a result of adverse pressure gradient, leading to undesirable contributions to the non-uniformity and unsteadiness at the contraction exit, weakening the effectiveness of the contraction ratio, see also Bell and Mehta [16]. It was therefore suggested by Morel [5] that to avoid flow separation, the contraction length is to be increased sufficiently, however, having a reasonable wall shape so that the boundary layer does not grow excessively near the contraction exit. Morel [5] recommended therefore that a contraction length ($L$) within the range $L = (0.75 - 1.25)D_i$ would be used in most of wind tunnels, where $D_i$ is the contraction base inlet diameter. A logical criterion for such a contraction length was the one related to the exit flow uniformity considerations, see e.g. Tsien [17], and Smith and Wang [18], to decide where the contraction contours should be terminated. In addition to the contraction length criteria, to optimize the profile of the contraction and examining its flow at both the inlet and exit, one would refer to few, however, comprehensive experimental, numerical, and analytical studies such as Morel [5,6], Lain and Harjumaki [20], Batill et al. [19], Tulapurkara and Bhalla [8], Callan and Marusic [9], and Abdelhamed et al. [3]. For examining flow at the contraction inlet, for instance, the maximum wall pressure coefficient ($C_{pi}$) was used as an indicator of the danger of flow separation at this end. On the other hand, the maximum wall pressure coefficient at the exit end ($C_{pe}$) was also used an indicator of the non-uniformity of the contraction exit flow.

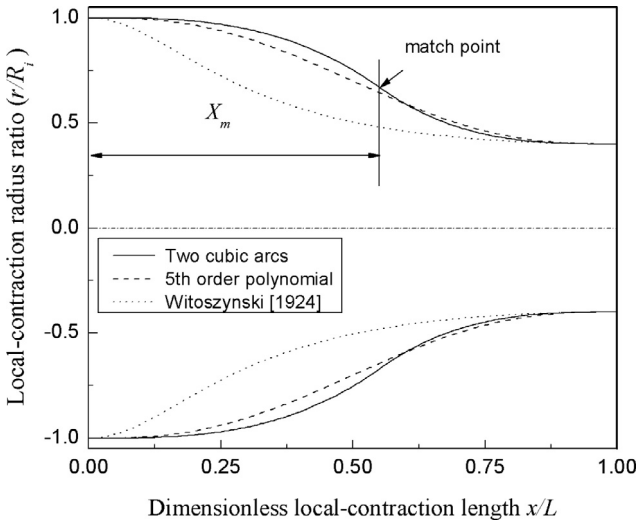


**Fig. 1** The wall contours of the three contractions under investigation.

Considerable efforts have recognized above, however, a controversy was observed about the contraction geometrical effects on contraction's flow quality. A proper selection for the contraction ratio, the contraction length, and the contraction-wall contour/shape is to be examined, motivating the present work.

To summarize, the most important criteria for a well-designed contraction are:

- Having uniform velocity profile at the contraction exit with low turbulence intensity level.
- Having flow free from separation for a minimum acceptable contraction length and hence minimum exit boundary layer thickness.

Before moving to the next section, a brief description of the manuscript is as follows. The numerical scheme, the experimental facility and the application of the measuring techniques utilized are introduced in Section 2. Section 3 presents the data computed and measured. Validation of the numerical results via the experimental data obtained from the experimental facility at LAS is carried out in Section 3. Finally, conclusions and final remarks are drawn and suggestions for further work are presented in Section 4. Hence, altogether the results presented in the present article provide a good insight into flow characteristics through low-speed wind tunnel contractions under study.

## 2. The numerical and experimental approaches

The numerical and experimental study proposed aimed at providing an answer for the contraction's geometrical effect on its flow quality. This is to be carried out via simulating numerically and validating experimentally contraction flow characteristics, in particular, in the contraction's core, near the wall, and at the exit plane where flow is emerging. Three wall contours for contractions tested have been prior selected. Fig. 1

represents the wall contours adopted for the three contractions investigated in the present study in normalized coordinates. It is worth noting here that the contraction ratio and length-to-inner diameter ratio are kept fixed for both the numerical simulations and experimental tests for all contractions. The wall shapes are defined as follows:

- The first contraction wall shape was defined by a 5th order polynomial:

$$r = a_0 + a_1 x + a_2 x^2 + a_3 x^3 + a_4 x^4 + a_5 x^5 \tag{1}$$

where $r$ is the local contraction radius, $x$ is the streamwise direction, $a_0, a_1, a_2, a_3, a_4, a_5$ are constants to be determined based on the inlet and outlet contraction's boundary conditions, i.e., at the contraction inlet, i.e. $x = 0:\ r = R_i,\ dr/dx = 0,\ \&\ d^2r/dx^2 = 0$, and at the contraction exit, i.e. $x = L:\ r = R_o,\ dr/dx = 0,\ \&\ d^2r/dx^2 = 0$, $i$ and $o$ refers to the inlet and exit contraction conditions.
- The second contraction wall shape was defined by two-matched cubic arcs:

$$r = (R_i - R_o)\left[1 - \left(\frac{1}{X_m}\right)^2 \left(\frac{x}{L}\right)^3\right] + R_0, \quad x/L \leqslant X_m \tag{2}$$

$$r = \frac{(R_i - R_o)}{(1 - X_m)^2}\left[1 - \left(\frac{x}{L}\right)^3\right] + R_0, \quad x/L \geqslant X_m \tag{3}$$

where $x/L$ is a dimensionless local-contraction length, and $X_m = x_m/L$ is the dimensionless contraction length where the matching of the two-cubic arcs occurs, see Figs. 1 and 2, see Hussain and Ramjee [7] for more details.
- The third contraction contour was defined by a 2nd order polynomial proposed by Witosznski [4] as follows:

$$r = \frac{R_o}{\sqrt{1 - \left[1 - \left(\frac{R_o}{R_i}\right)^2\right]\left[\frac{\left(1 - \frac{3x^2}{L^2}\right)^2}{\left(1 + \frac{x^2}{L^2}\right)^3}\right]}} \tag{4}$$

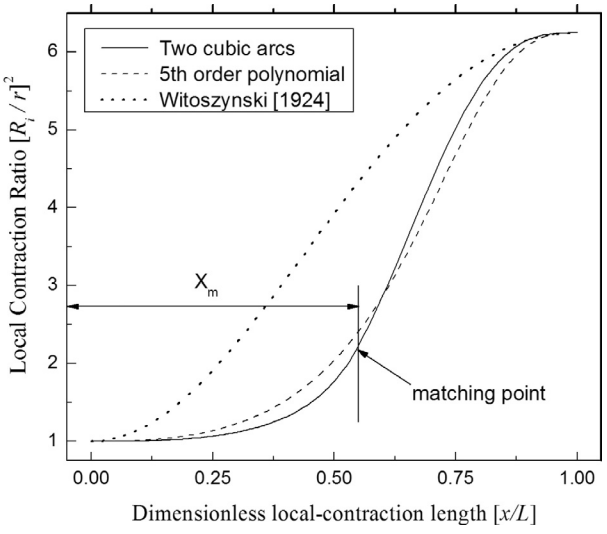


**Fig. 2** The rate of change of the local wall-shape parameter $(R_i/r)^2$ versus the normalized contraction length $(x/L)$ for the three contractions under investigation.

To simplify the analysis of the contraction problem, the most relevant design parameters considered are summarized in a functional relationship as follows:

$$(u_c')\ and/or\ (\Delta U) = f(\overline{U}_c, r, R_i, R_o, L, \rho, \mu), \tag{5}$$

where $u_c'$ is the centerline velocity fluctuation at the contraction exit plane, $\Delta U = (\overline{U} - \overline{U}_c)$ is the non-uniformity measure of the mean velocity profile at contraction exit, $\overline{U}_c$ is the average centerline flow velocity at the contraction exit plane, $r$ is the local contraction radius, $R_i$ & $R_o$ stand for the contraction inlet and exit radii, $L$ is the contraction entire length, $\rho$ is the fluid density, and $\mu$ is the fluid dynamic viscosity.The dimensional analysis of the above functional relationship proposes the following dimensionless relation:

$$\frac{u_c'}{\overline{U}_c}\ and/or\ \frac{\Delta U}{\overline{U}_c} = f\left[Re_c, \left(\frac{R_i}{R_o}\right)^2, \left(\frac{R_i}{r}\right)^2, \left(\frac{L}{R_i}\right)\right], \tag{6}$$

where $(u_c'/\overline{U}_c)$ is the centerline turbulence intensity at the contraction exit plane, $(\Delta U/\overline{U}_c)$ is the dimensionless non-uniformity measure of the mean velocity profile at the contraction exit plane, $Re_c = \overline{U}_c D_o/\nu$ is the centreline-mean-based Reynolds number, $(R_i/R_o)^2$ is the contraction ratio $(CR)$, $(R_i/r)^2$ represents the local wall shape parameter of the contraction, and $(L/R_i)$ is the contraction length to the inlet contraction radius ratio.Since the contraction ratio and the contraction length-to-inner diameter ratio are kept fixed in the present study, Eq. (6) can be re-written as follows:

$$\frac{u_c'}{\overline{U}_c} \quad or \quad \frac{\Delta U}{\overline{U}_c} = f\left[Re_c, \left(\frac{R_i}{r}\right)^2\right], \tag{7}$$

Eq. (7) indicates that contractions with fixed contraction ratio and having similar normalized contraction length will have flow quality and/or non-uniformity that depend mainly on the Reynolds number $(Re_c)$ and the local wall-shape parameter $(R_i/r)^2$.

In addition to flow non-uniformity, another dimensionless number of considerable importance for characterizing flow separation is the mean-pressure coefficient defined at both the contraction inlet $(C_{pi})$ and exit $(C_{po})$ planes, respectively, as follows:

$$C_{pi} = 1 - \left(\frac{\overline{U}_i}{\overline{U}_{ci}}\right)^2, \quad C_{po} = 1 - \left(\frac{\overline{U}_o}{\overline{U}_{co}}\right)^2, \tag{8}$$

It is worth re-noting that the geometrical parameters, i.e. $(CR)$ and $(L/R_i)$, for all three contractions presented in Figs. 1 and 2 are similar. The present results showed strong dependence of both $(\Delta U/\overline{U}_c)$ and $C_p$ on the contraction wall contour as will be shown later in details in Section 3.

Fig. 2 represents the local contraction ratio $C = (R_i/r)^2$ versus the normalized contraction length $(x/L)$. One might observe from this figure that the rate of change of the local contraction ratio, i.e. $dC/d(x/L)$, at the contraction inlet is abrupt for the Witoszynski 2nd order polynomial contraction. The two-cubic arcs and the 5th order polynomial look to some extent similar, however, deviate clearly from the Witoszynski contraction. The rapid change in the Witoszynski 2nd polyno-

mial contraction at inlet might result in an early flow separation at its inlet in contrast to the other two contractions, this will be shown later. The next subsection highlights details of the main features of both the numerical and experimental approaches applied to predict flow characteristics through contractions under study.

### 2.1. The numerical scheme

In boundary layer theory, the presence of a thin boundary layer, i.e. $\delta^*/R \ll 1$, does not change the potential flow pressure distribution, particularly, in the core region of the contraction, here $\delta^*$ stands for the boundary layer displacement thickness. This condition is well satisfied in most of the wind tunnel applications, see Morel [5], and therefore, the potential flow assumption in the current numerical simulation is justified, see also Lain and Harjumaki [20]. The present numerical simulations, therefore, used 2D, axisymmerty, finite volume (AnsysFluent 14.5) software. An inviscid/potential, pressure-based segregated flow solver was utilized to calculate the pressure and the velocity distributions along the core, and near the wall of each contraction under investigation. In addition, few simulations with viscous flow solver, Spalart-Allmaras model, were carried out and compared to inviscid simulations, demonstrating that the inviscid/potential approach was indeed sufficient. It is also worth noting that a second-order upwind discretization scheme for momentum was implemented.

The computational domain for each contraction considered in this piece of work is presented in Fig. 3, showing the second grid level for the present numerical analysis. The computational domain is meshed using a quadrilateral cells. The mesh of the second grid level shown in Fig. 3 has 128,000 elements with a minimum orthogonal quality 7.80086e−01 and maximum aspect ratio 3.24247e+01. All contractions have similar inlet and outlet diameters as well as contraction length, however, having three various wall contours as shown earlier in Figs. 1 and 2. The contraction ratio $(R_i/R_o)^2$ is 6.25, and the contraction length to the inlet diameter ratio is 1, i.e. $L/2R_i = 1$. Due to the contraction symmetry, only half of the contraction was simulated numerically. The boundary conditions applied for the numerical flow investigations are shown in Fig. 3. At the inlet (i.e. the contraction's left side), a uniform velocity profile has been described. A zero normal gradient boundary condition was set for all parameters at the outlet (i.e. the contraction's right side). The centerline was modeled as a symmetry line and the confining upper boundary was modeled as a wall where the no-slip boundary condition is automatically assigned. To validate the numerical results, experimental data have been obtained utilizing the aeroacoustic test facility available at LAS BTU-Cottbus Senfttenberg with contractions geometrically similar to those numerically simulated.

### 2.2. The experimental approach

Experimentally, a low speed aeroacoustic facility at the Department of Aerodynamics and Fluid Mechanics (LAS), BTU-Cottbus-Senftenberg, has been utilized for experiments. The aeroacoustic test facility, see Fig. 4, is laid out openly, i.e. free jet without direct feedback. The facility uses a radial fan to provide air with 60 m/s maximum velocity at the nozzle exit plane. The facility flow rate and consequently the Reynolds number for each investigated case were controlled by changing the rotational speed of a 5.5 kW radial fan via a fre-

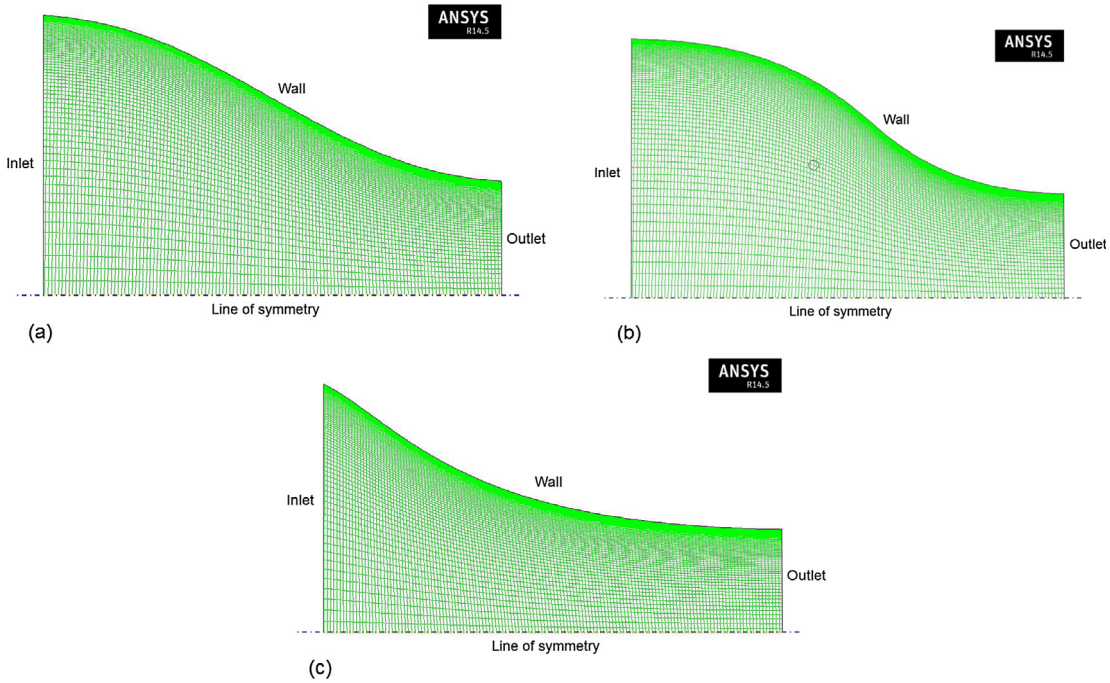


**Fig. 3** The geometries and computational second grid level for all three contractions under investigation: (a) 5th order polynomial, (b) two-cubic arcs, (c) 2nd order polynomial [4].

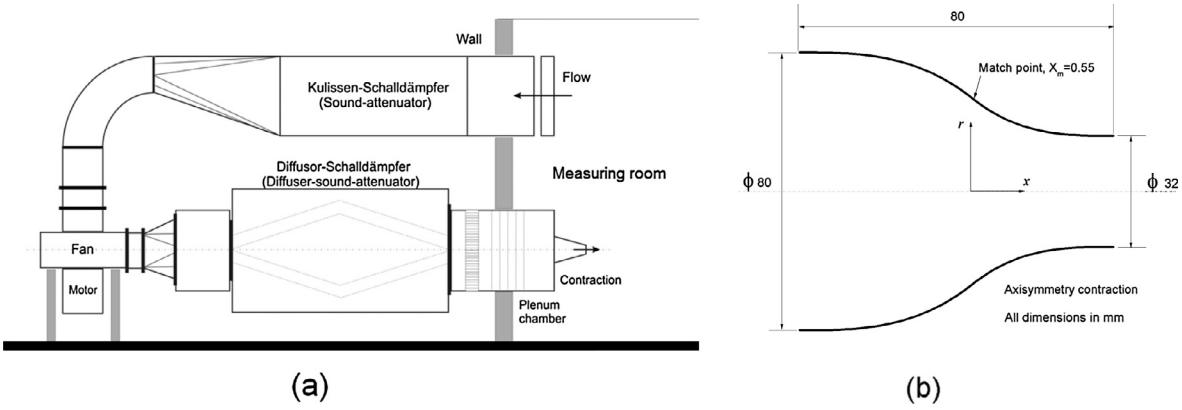


**Fig. 4** (a) Schematic of the aeroacoustic tunnel facility at LAS BTU, and (b) Dimensional two-Cubic arcs contraction.

quency converter unit. To carry out the present experimental work, three contractions were connected directly, however, separately in a sequential manner to the plenum chamber of the experimental facility in the measuring room, see Fig. 4. All contraction sections are symmetric, having a contraction ratio of 6.25, carefully machined and made out of smooth PVC. The base diameter of the contraction is 80 mm, the outlet diameter is 32 mm and the total length is 80 mm, see Fig. 4b. DANTEC constant-temperature anemometer (Multi-channel CTA System) was used to measure the turbulence intensity level at the centerline of the exit plane of each contraction. The hot-wire measurements of the local velocity were made utilizing a boundary layer probe equipped with a 5 μm diameter wire ($d$) and 1.25 mm an active wire length ($\ell$), providing an aspect ratio ($\ell/d$) of 250. Hence the wire had a sufficiently large aspect ratio to suggest a negligible influence of the prongs on the actual velocity measurement. Calibrations and measurements were performed with an 80% overheat ratio, $a = (R_w - R_a)/R_a$, where $R_w$ is the operational hot-wire resistance and $R_a$ is the resistance of the cold wire, i.e. at ambient air temperature. For the statistical data analysis of the local flow, $5 \cdot 10^4 - 10^5$ samples were acquired over 60 s at every measuring location.

Intensive measurements of the mean velocity profiles, the bulk flow velocity, the centerline average velocity, and the centerline velocity fluctuations were made at the contraction exit plane for various Reynolds numbers. The centerline turbulence intensity level was found to be less than 0.5%, see Fig. 5. Fig. 5 represents the centerline turbulence intensity level measured at the exit plane of (a) the 5th order polynomial, (b) the two-cubic arcs and (c) Witoszynski 2nd order polynomial contractions for various Reynolds numbers. Monotonic decrease for the turbulence intensity, $u'/U_c$, versus the Reynolds number was observed, see Zanoun et al. [21] for more details. Data scatter might be observed in Fig. 5, however the low level of the exit velocity fluctuations, i.e. $u'/U_c \leq 0.5\%$, shown in the figure suggests a laminar flow at the contraction exit. The scatter observed might be attributed to the not large enough total number of samples or to the short length of the sampling time.

In addition to the hot wire, a conventional one-dimensional laser-Doppler anemometry (LDA), DANTEC Flowlite, operating in dual-beam, back-scattering mode was used to conduct more measurements at the contraction exit plane. The dimensions of the LDA control volume ($dx \times dy \times dz$) are $0.074 \times 0.074 \times 0.554$ mm$^3$. A two-dimensional traversing mechanism (ISEL) having step size from 0.02 mm to 5 mm was used to traverse the LDA control volume in both $y$ and $z$ directions. A particle generator (Atomizer Aerosol Generator, AMT 230) was used to produce liquid particles with mean diameter $\leqslant 1$ μm for seeding the air flow. The liquid particles were introduced upstream the plenum chamber to ensure well particle distribution before reaching the contraction exit plane. Depending on the mean flow velocity and particles concentration, data rates of 100–3000 Hz were typically obtained. For computing the local mean velocity, 20000 samples were acquired at every measuring location.

The bulk flow velocity, $\overline{U}_b$, was estimated at the contraction exit where a uniform velocity distribution is expected or by integrating the mean velocity profile measured at the exit plane for each running case. It was then used to calculate the bulk-velocity based Reynolds number of the flow, $Re_m = \overline{U}_b D/\nu$. A low range of Reynolds numbers, i.e. $Re_m \leqslant 106 \cdot 10^3$ which was corresponding to a bulk velocity $\leqslant$50 m/s, was set up in this way. The LDA measurements have been carried out at around 40 vertical and/or horizontal locations across the contraction exit plane with particular attention being given to:

- The bulk flow velocity ($\overline{U}_b$) and the centerline average velocity ($\overline{U}_c$)
- The centerline turbulence intensity level ($u'_c/\overline{U}_c$)
- The mean velocity distributions, i.e. $\overline{U} = f(y)$.

## 3. Results and analysis

It is commonly believed that the numerical simulation is never trusted unless the solution is grid converged to an acceptance level of tolerance and/or compared with accurate experimental data. In Fig. 6, numerical results from both the first and the second grid levels are presented. The figure shows close agreement between the numerical results received from both the first and the second grid levels. In addition, the good agreement of the simulations with the experimental data, see Fig. 7, led to no further mesh refinement. It is worth re-noting that numerically, inviscid as well as viscous flow solvers were utilized for computing the mean flow parameters. Fig. 7(a) illustrates the mean pressure coefficient and 7(b) shows the normalized velocity

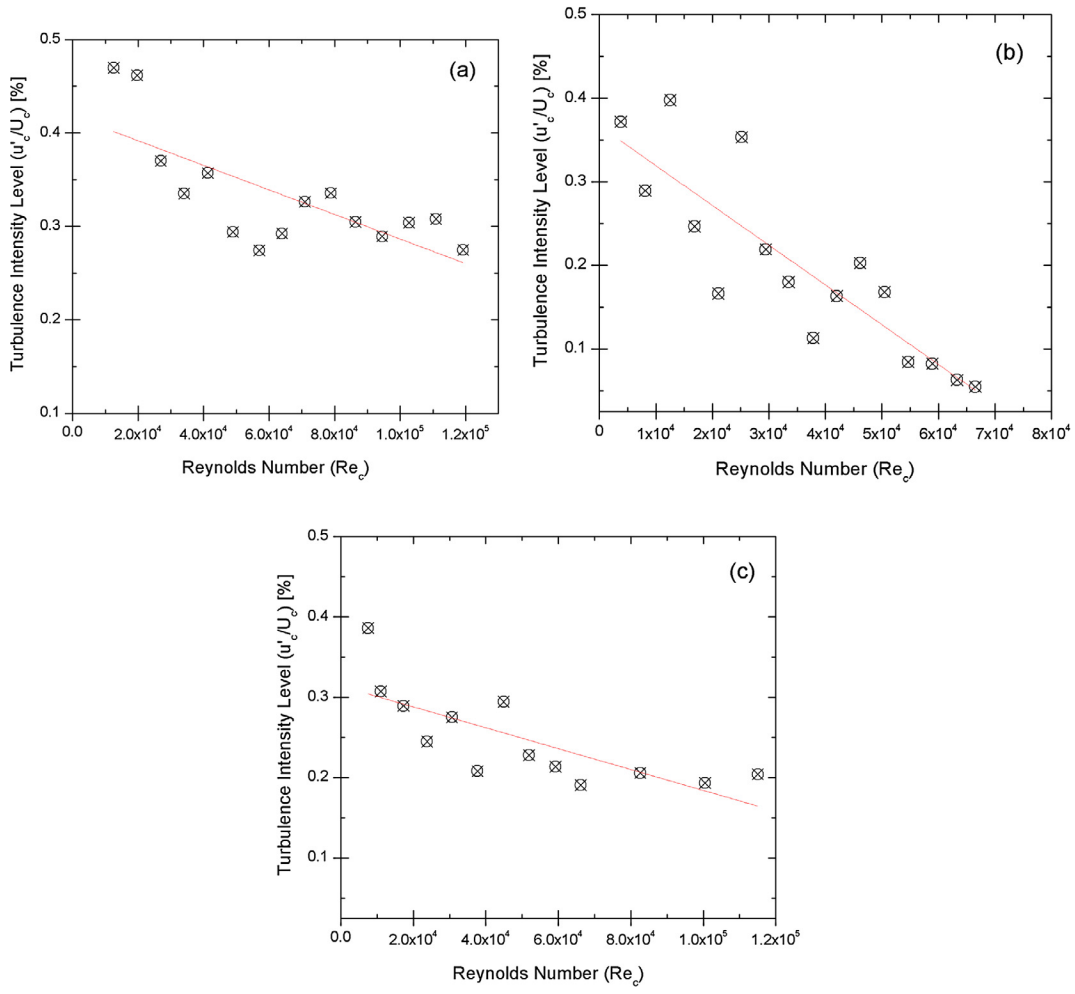


**Fig. 5** The centerline turbulence intensity level measured by the hot-wire anemometry at the exit plane of (a) 5th order polynomial, (b) two-cubic arcs, and (c) Witoszynski 2nd order polynomial contractions.

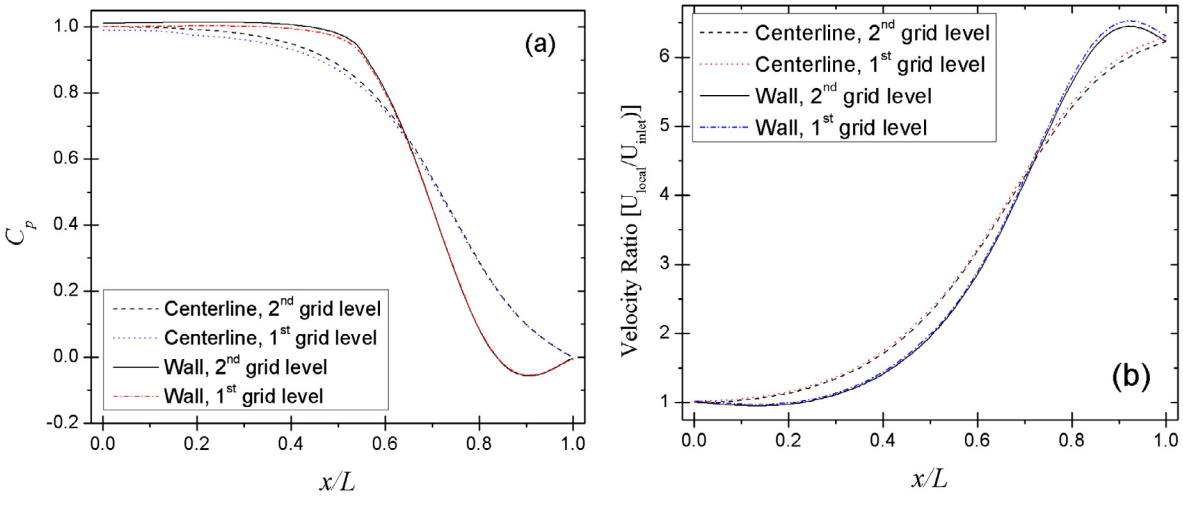


**Fig. 6** (a) The mean pressure coefficient, $C_p$, and (b) normalized velocity, $U_{local}/U_{inlet}$, predicted for two different grid levels along the 5th order polynomial contraction's centerline and wall layer versus the normalized streamwise distance $(x/L)$ for $Re_c \approx 33 \times 10^3$.

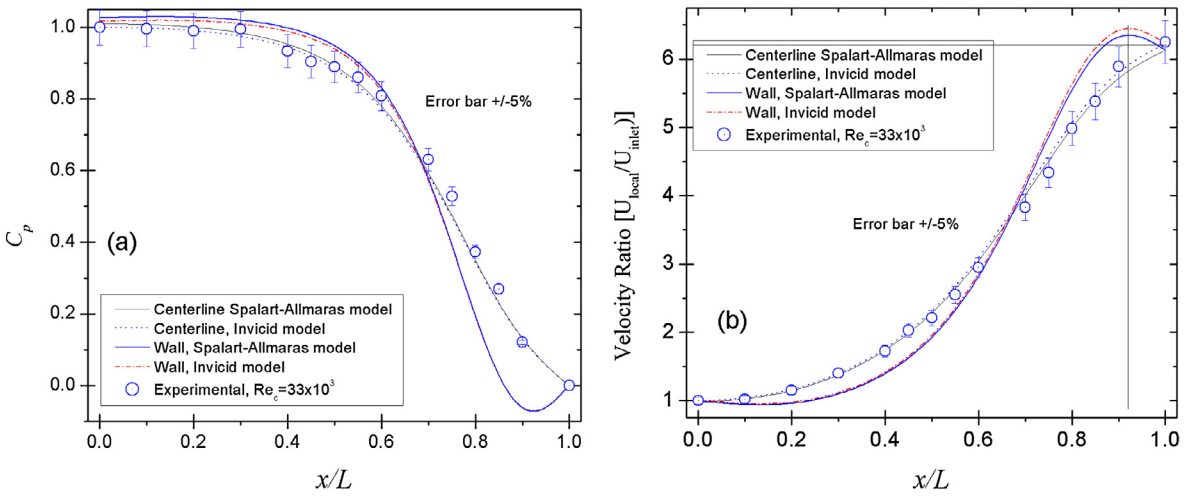


**Fig. 7** (a) The mean pressure coefficient, $C_p$, and (b) normalized velocity, $U_{local}/U_{inlet}$, predicted utilizing viscous and inviscid models along the 5th order polynomial contraction's centerline and wall layer versus the normalized streamwise distance $(x/L)$ for $Re_c \approx 33 \times 10^3$ compared to experimental data.

predicted along the centerline and in immediate vicinity of the wall for the 5th-order polynomial contraction, utilizing both the inviscid/potential and viscous/Spalart-Allmaras model. Comparable results in Fig. 7 are obtained and one hardly observes the difference between the results obtained using both models. The figure demonstrates, therefore, that the inviscid/potential approach is indeed sufficient as discussed earlier in Section 2.1. Hence, the AnsysFluent potential flow solver was mainly used for results presented thereafter.

### *3.1. The numerical and experimental pressure data*

An earlier design methodology for the contraction was to define a velocity distribution at its centerline and then to calculate a set of stream surfaces from it, and thereafter the corresponding wall shape was to be defined, see e.g. Tsien [17], Szczeniowski [22], Thwaites [23] and Bloomer [24], Cohen and Ritchie [25]. On contrary, what has been adopted in the present work was that predicting and measuring the velocity and the pressure fields for a pre-selected contraction wall shape. Experimentally as well as numerically, at the contraction entry a uniform flow originating from stagnation conditions was assumed and its development was followed throughout the contraction passage. A comparison was then carried out between the numerically predicted flow data at the contraction exit plane against the data measured utilizing the experimental facility with the LDA. The first set of data predicted numerically is the mean pressure coefficient, $C_p = (P - P_\infty)/(1/2\rho U^2)$, calculated along the contraction centerline and on the wall vicinity for all three contractions under study.

Selected samples of the $C_p$ data for the 5th polynomial, two-cubic arcs and Witoszynski 2nd order polynomial contractions are presented in Figs. 8 and 9 for $Re_c = 25800$. Close to the contraction entry, i.e. $x/L < 0.5$, for both the 5th order polynomial (Fig. 8a) and the two-cubic arcs (Fig. 8b) an almost constant behavior for the mean pressure coefficient was observed with slightly higher values along the wall when compared to those along plane of symmetry/centerline. This is attributed to the fact that flow is being accelerated more along the centerline. Downstream of $x/L > 0.5$, a monotonic decrease in the mean pressure coefficient with steeper slope was observed, in particular, along the wall as compared to the corresponding values along the centerline for both the 5th order polynomial (Fig. 8a) and the two-cubic arcs (Fig. 8b) contractions. On the contrary, changes in the mean pressure coefficient starts early very close to the entry of the Witoszynski 2nd order polynomial contraction with noticeable higher values along the wall layer when compared to those on the contraction centerline for $x/L < 0.4$, while an opposite character is observed for $x/L > 0.4$. In Fig. 8a and b, the slightly lower values for the mean pressure coefficient observed for $x/L > 0.65$ along the wall are due to the streamwise and radial negative pressure gradients obtained, see both Figs. 10 and 11, accelerating the flow along the wall layer. This results in undershoot in the mean pressure coefficient close to the contraction exit, i.e. velocity overshoot as will be shown later in Fig. 13. Similar behavior was obtained for flow in the Witoszynski 2nd order polynomial contraction for $x/L > 0.4$, see Fig. 8c.

Differences among the Witoszynski 2nd order polynomial and the other two contractions are pronounced in Fig. 9. Having a closer look at data presented in Fig. 9, one could clearly observe good agreement between the $C_p$ rate of change (i.e. $dC_p/d(x/L)$) for the 5th order polynomial and the two-cubic arcs either along plane of symmetry (Fig. 9a) or along the contraction's wall (Fig. 9b). The slope of the $C_p$ along the centerline for $0.4 < x/L < 0.7$ is, however, approximately the same for all three contractions under investigation. On the other hand, close to the contraction inlet, i.e. for $x/L < 0.4$, a rapid change in the local centerline pressure coefficient magnitudes is to be observed for the Witoszynski 2nd order polynomial when compared with the two-cubic arcs as well as with the 5th order polynomial. A similar wall pattern is observed along the centerline for the Witoszynski 2nd order polynomial, however, close to its inlet a narrow localized region of higher wall pressure coefficient values was observed in Fig. 9(b) compared to both the 5th order polynomial and the two-cubic arcs values.

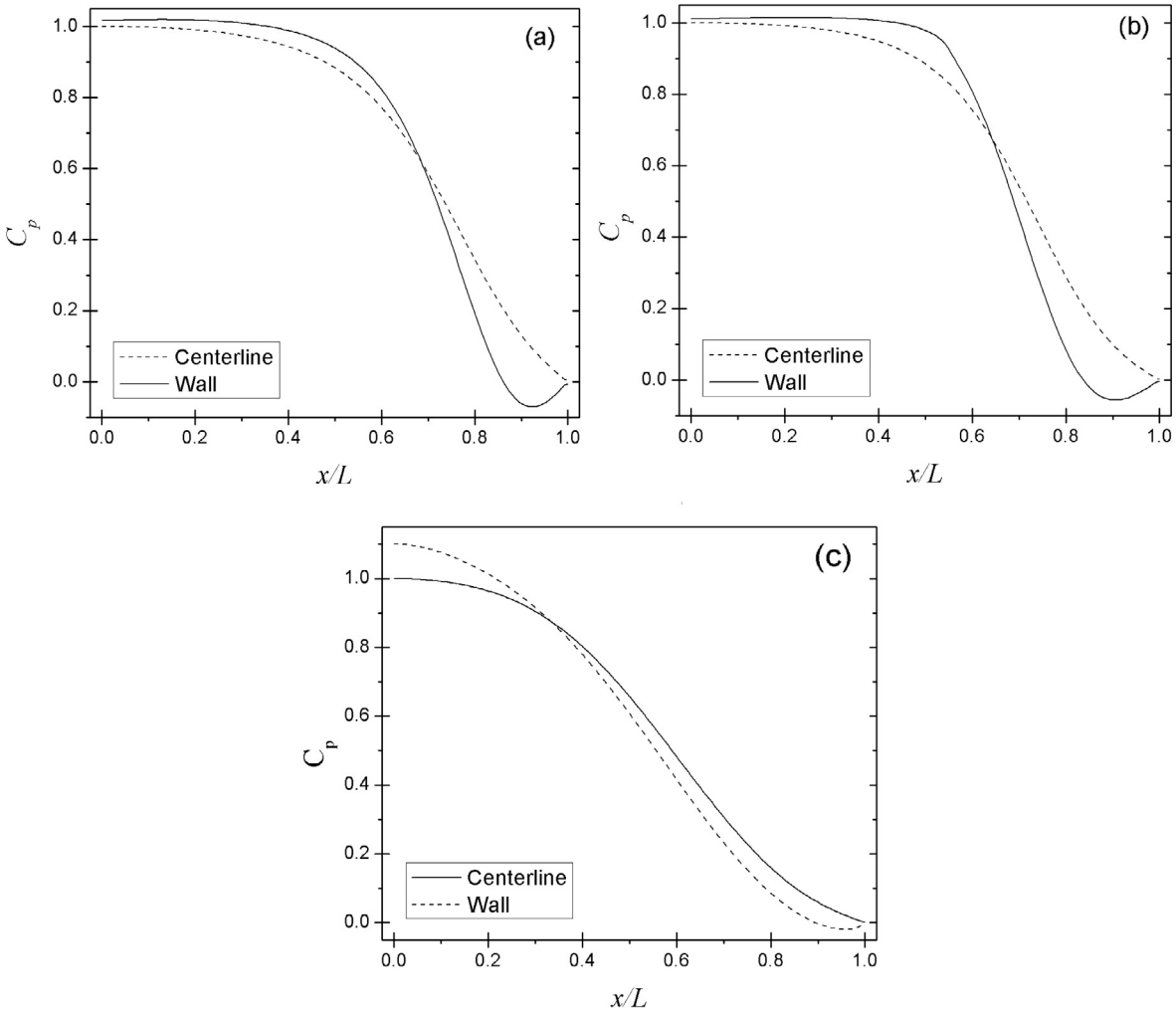


**Fig. 8** The mean pressure coefficient predicted along the walls and the centerlines for (a) 5th order polynomial contraction, (b) two-cubic arcs contraction, (c) Witoszynski 2nd order polynomial contraction for $Re_c = 25800$ versus the normalized streamwise distance $(x/L)$.

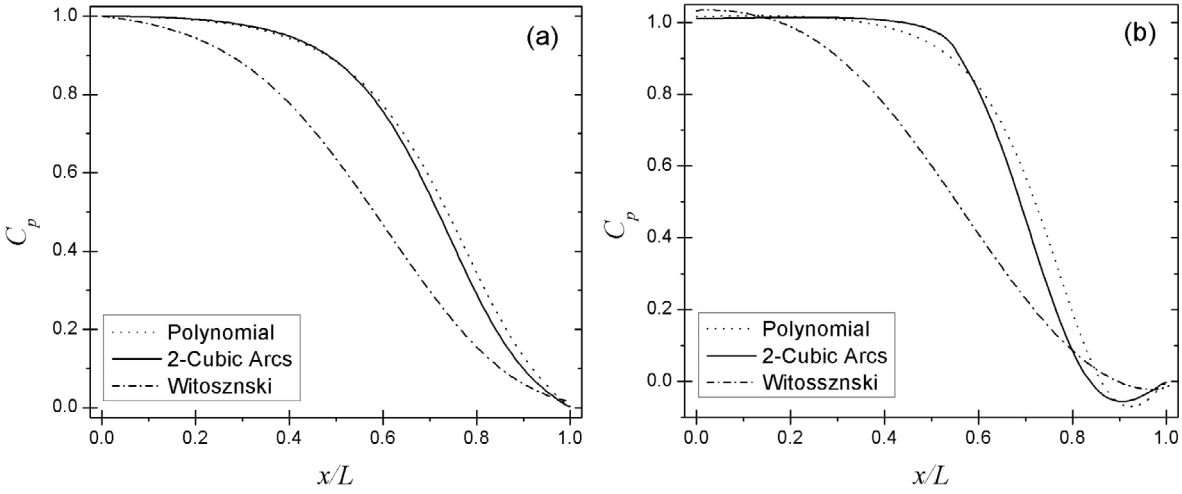


**Fig. 9** Comparison of the mean pressure coefficient predicted along (a) the contraction centerline/plane of symmetry, (b) the contraction wall versus the normalized streamwise distance $(x/L)$ for $Re_c = 25,800$.

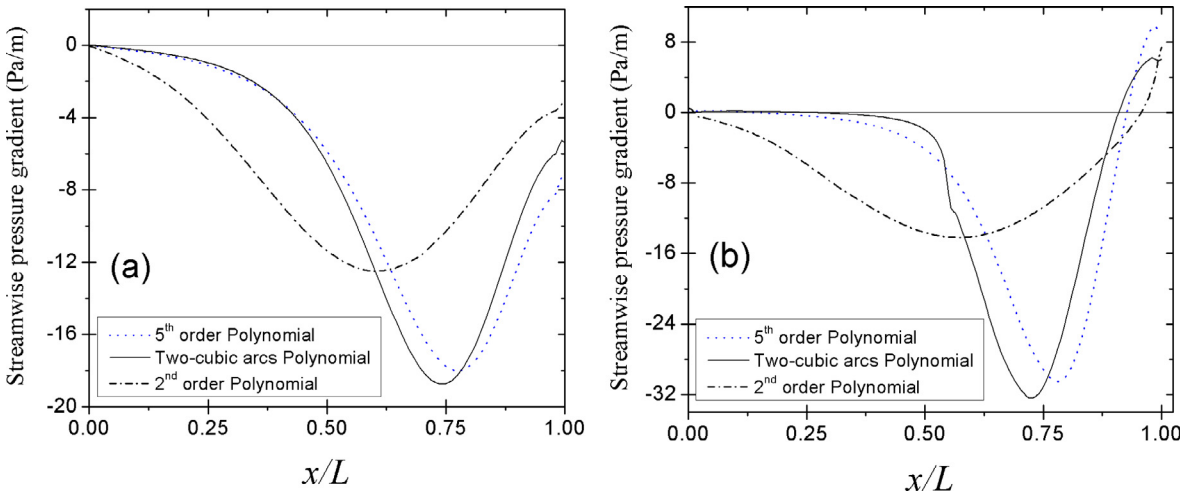


**Fig. 10** The predicted streamwise pressure gradient ($dp/dx$) for all contractions along (a) the centerlines, (b) the walls for $Re_c = 25,800$.

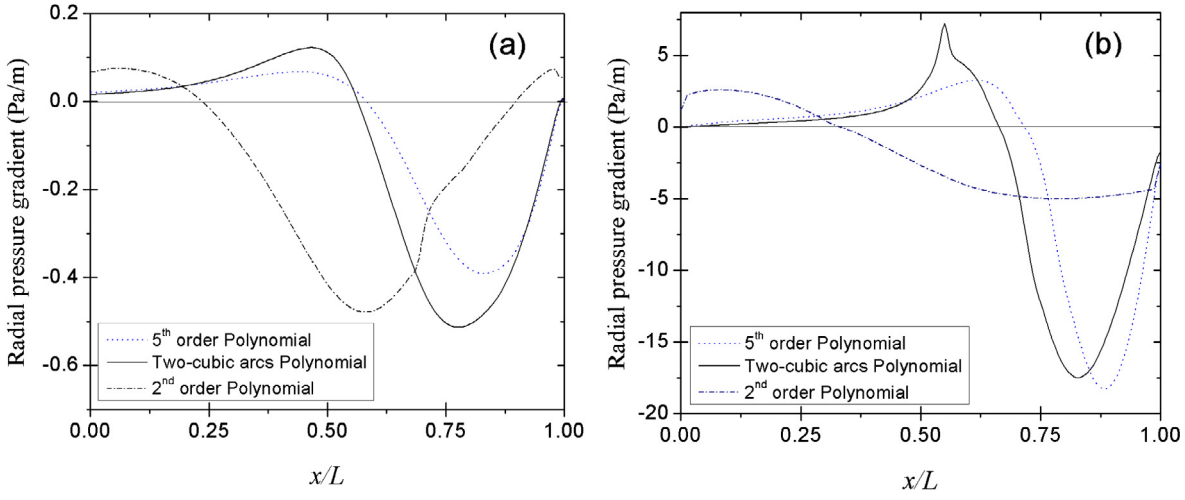


**Fig. 11** The predicted radial/wall-normal pressure gradient ($dp/dr$) for all contractions along (a) the centerlines, (b) the walls for $Re_c = 25,800$.

The local higher values for the wall mean pressure coefficient near the inlet plane, i.e. $x/L < 0.2$, for the Witoszynski 2nd order polynomial contraction shown in Fig. 9b, indicates flow tendency to separate at its inlet plane. This could be attributed to the positive radial pressure gradient observed close to the inlet boundary layer shown in Fig. 11b, resulting in pressure variation across the boundary layer in radial direction. This leads to centrifugal instability (Görtler instability) of the boundary layer and consequent formation of Görtler vorticies, and therefore, tendency of the flow to separate, see Floryan [26]. It is, however, generally believed that the boundary layer is less subjected to separation close to the exit due to the favorable streamwise and radial pressure gradients exited as shown in Figs. 10 and 11, respectively, see also Morel [5]. Fig. 10a and b illustrates the predicted streamwise pressure gradient ($dp/dx$) for all contractions along the centerlines, Fig. 10a, and the walls, Fig. 10b, for $Re_c = 25800$. One might observe similar flow behavior for both the 5th order polynomial and the two-cubic arcs contractions either along the walls or along the centerlines. Weak unfavorable, i.e. positive, streamwise pressure gradient along walls was observed for $x/L > 0.9$ for

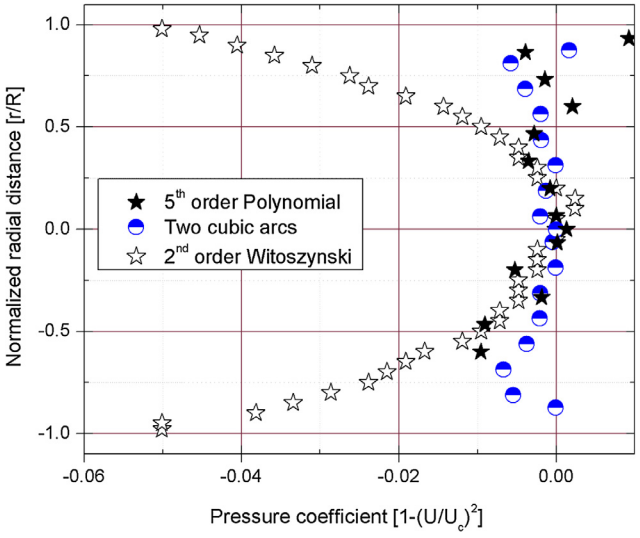


**Fig. 12** The normalized experimental pressure coefficient along all contractions exit planes for $Re_c = 25,800$.

all three contractions in Fig. 10b. On the other hand, in Fig. 11b favorable radial pressure gradients with higher values was observed along walls around $x/L = 0.9$, in particular, for both the 5th order polynomial and the two-cubic arcs contractions. Hence, the negative radial pressure gradient close to the exit plane dominates, resulting in velocity overshoots in velocity profiles along both the walls of both contraction, see Fig. 13a and b. In Fig. 11b, one might observe also very weak unfavorable radial pressure gradient around the middle of both the 5th order polynomial and the two-cubic arcs contractions on contrary to the streamwise favorable mean pressure gradient shown in Fig. 10. Therefore, on the core part of both contractions the streamwise favorable mean pressure gradient dominates the flow, preventing flow separation.

Experimentally, the mean pressure coefficient was estimated close to the contraction exit via the mean velocity measurements utilizing the LDA and the results obtained are presented in Fig. 12. Based on the experimental data a similar behavior of the mean pressure coefficient along the contraction exit plane, particularly, around the centerline to those predicted numerically was observed in Fig. 12 for all contractions under study. At the contraction center, an almost zero pressure coefficient was obtained experimentally and this turns out to be in agreement with the numerical predictions in Fig. 8. Slightly off the contraction centerline, the mean pressure coefficient was found to be around $-0.01$ for either the 5th order polynomial or the two-cubic arcs, clarifying the tendency of flow to accelerate without separation at the exit. However, higher negative pressure coefficient values were obtained experimentally away from the centerline at the exit plane of the Witoszynski 2nd polynomial contraction, resulting in more flow acceleration at the Witoszynski's contraction exit plane.

### 3.2. The numerical and experimental velocity data

In this subsection, the predicted and measured mean velocity profiles for various Reynolds numbers along the core, in wall proximity, and at the exit plane for all contractions under investigation have been presented in Figs. 13–18. Numerically, at the contraction inlet, a uniform velocity profile, originating

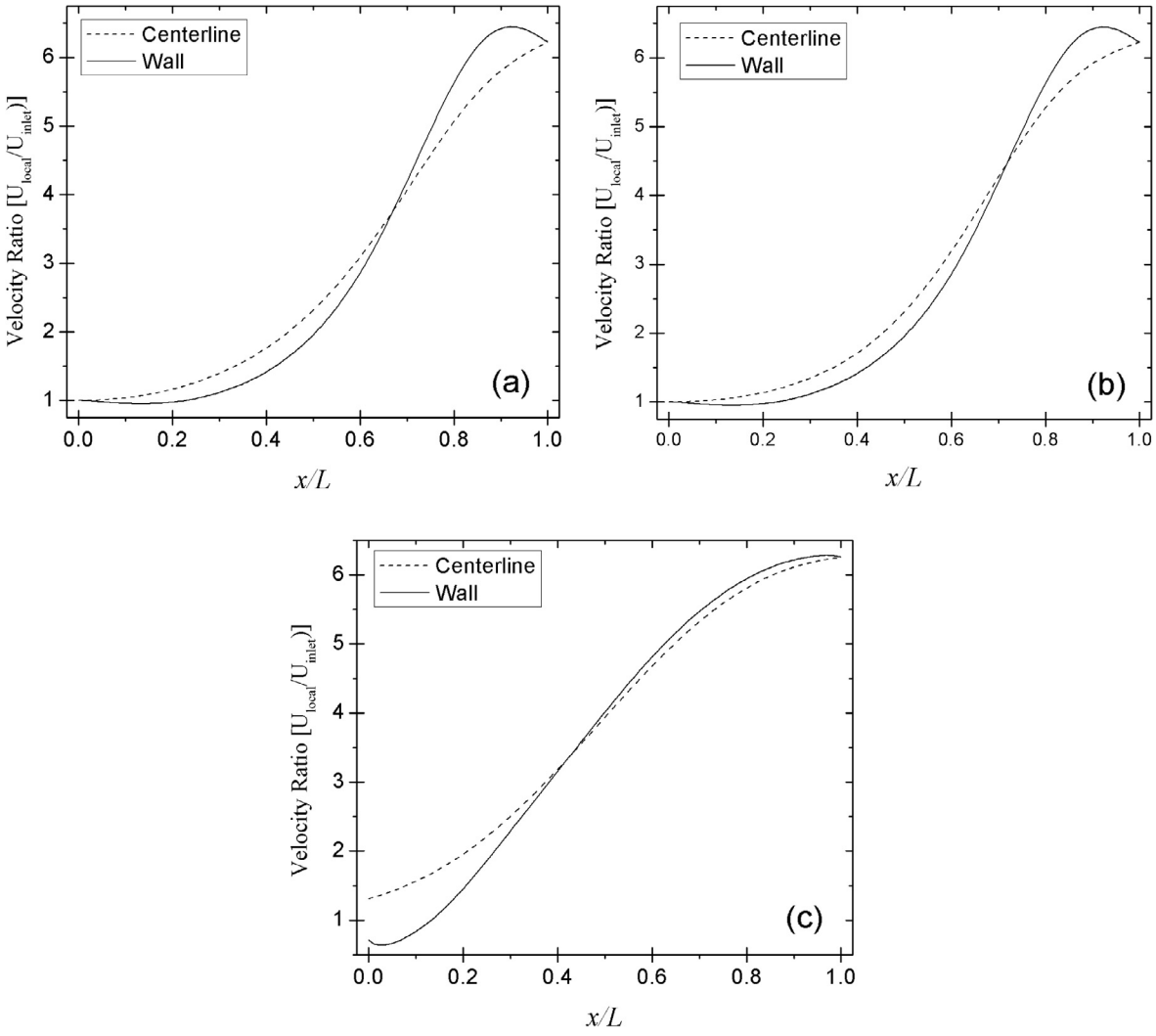


**Fig. 13** The mean normalized velocity, $U_{local}/U_{inlet}$, calculated along the contraction wall layer and plane of symmetry/centerlines for (a) 5th order polynomial, (b) two-cubic arcs, (c) 2nd order Witoszynski contractions versus the normalized streamwise distance $(x/L)$ for $Re_c = 25,800$.

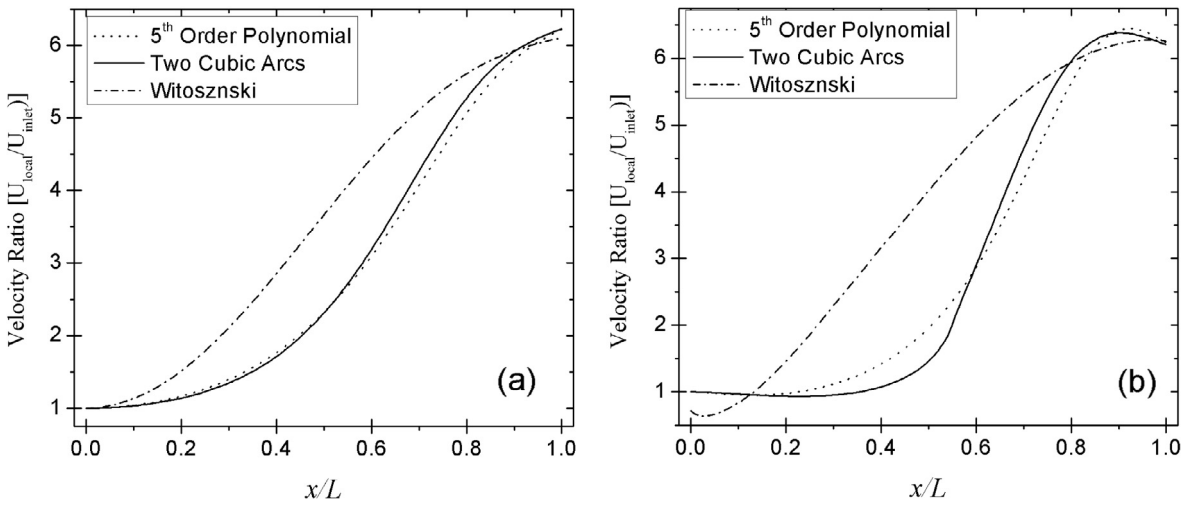


**Fig. 14** Comparison of the normalized mean velocity, $U_{local}/U_{inlet}$, predicted along (a) the contraction plane of symmetry/centerline, (b) the contraction wall versus the normalized streamwise distance $(x/L)$ for $Re_c = 25,800$.

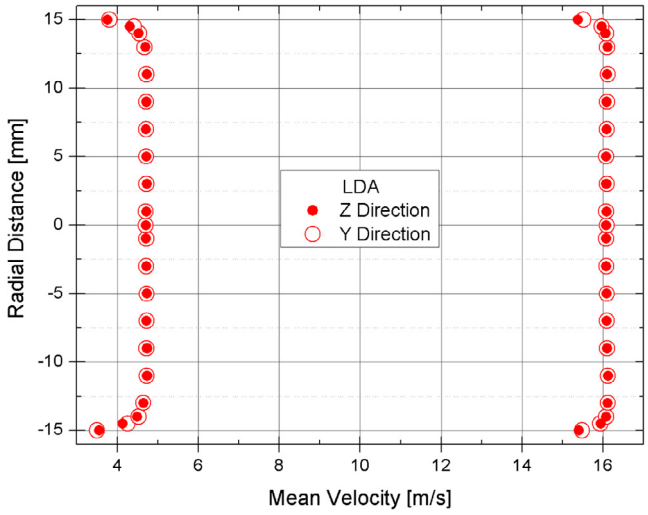


**Fig. 15** The measured mean velocity profiles at the exit plane of the 5th order polynomial contraction for two different Reynolds numbers, $Re_c = 10^4$ and $Re_c = 33 \times 10^3$ utilizing the LDA in wall-normal (y) and spanwise (z) directions.

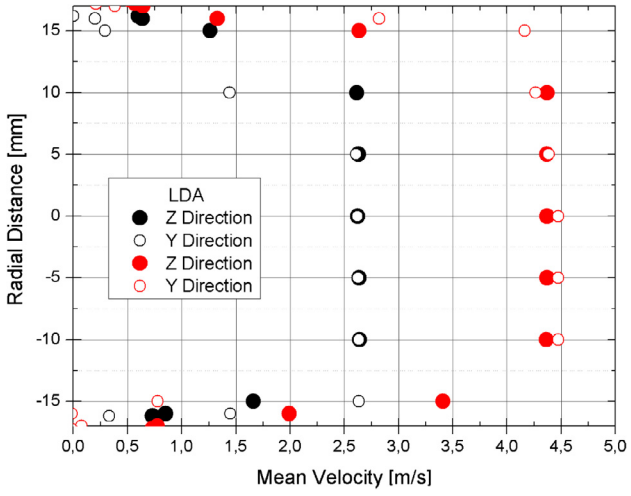


**Fig. 16** The measured mean velocity profiles at the exit plane of the two-cubic contraction for two different Reynolds numbers, $Re_c = 5.5 \times 10^3$ and $Re_c = 9.3 \times 10^3$ utilizing the LDA in wall-normal (y) and spanwise (z) directions.

from stagnation condition has been described and its development along the contraction length was observed. Selected samples of the numerical velocity profiles are presented in Figs. 13 and 14 for $Re_c = 25,800$. In all cases, one might observe either from Fig. 13 or Fig. 14 a monotonic increase in the mean velocity along the wall layer as well as the plane of symmetry/-centerline of the contraction, however, with different rates. Along contraction's plane of symmetry/centerline and the wall layer, flow accelerates in a normal manner, however with different rates according to the wall contour as Figs. 13 and 14 illustrate. Earlier, it was observed in Fig. 7 that close to the contraction entry the $C_p$ values along the wall are slightly higher than those along the plane of symmetry for $x/L < 0.5$, resulting in higher centerline velocities than those along wall layer as Figs. 13 and 14 show. A local minimum velocity along the wall layer near the inlet of the Witoszynski 2nd order polynomial contraction, i.e. $x/L < 0.15$ was observed in Fig. 13c. This is attributed to the rapid change in wall curvature, see Fig. 2, and therefore to the transverse/radial adverse pressure gradient, $dp/dr$, that dominates the inlet plane of the Witoszynski 2nd order polynomial contraction as Fig. 11b showed. Near the contraction exit, i.e. around $x/L = 0.9$, of both the 5th order polynomial and the two cubic arcs, the near-wall velocity is observed to be higher than the velocity at the plane of symmetry by around 5% maximum, see Fig. 13a, b and Fig. 14b. This might be attributed to the wall curvature and therefore to the negative pressure values presented in Figs. 9b and 11b. However, the velocity overshoot observed in either the 5th order polynomial or the two cubic arcs contractions lies within the tolerance level, i.e. $\leqslant 10\%$ in

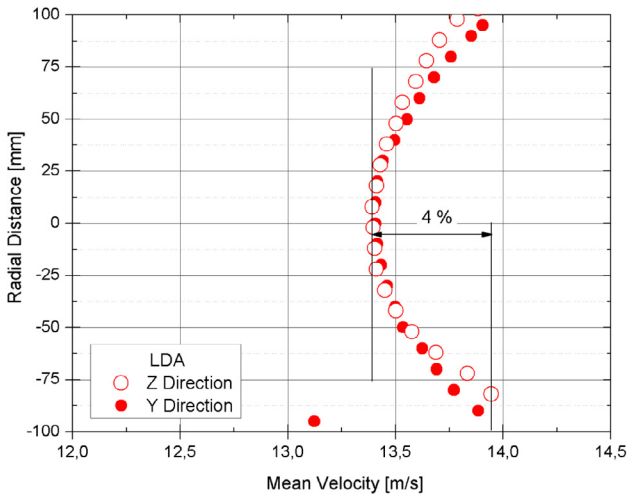


**Fig. 17** The measured mean velocity profiles at the exit plane of the 2nd order Witoszynski contraction for Reynolds number of $Re_c = 28 \times 10^3$ utilizing the LDA in wall-normal (y) and spanwise (z) directions.

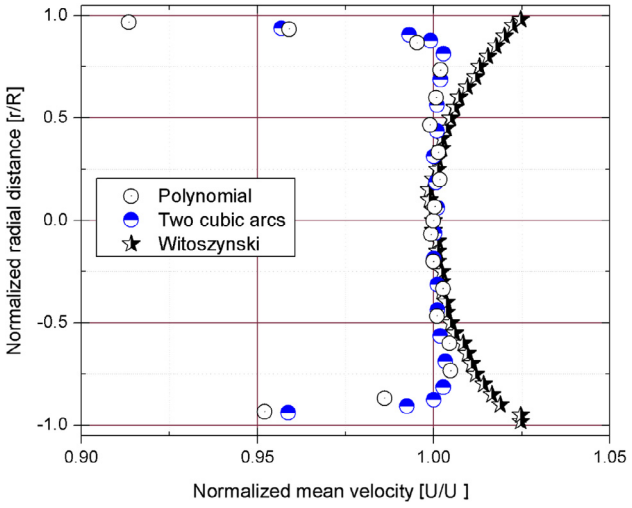


**Fig. 18** A comparison of the measured normalized mean velocity profiles for the 5th order polynomial, the two-cubic arcs and the Witoszynski 2nd order contractions for almost the same Reynolds number.

wind tunnel applications as indicated by Morel [5]. The validation of the numerical results was carried out by comparing the numerical data with data from contraction sections tested on the aeroacoustic facility. The Laser Doppler was used to measure the mean velocity at various locations close to the exit plane for each contraction. Samples of the mean velocity profiles measured were presented in Figs. 15–18. The experimental results shown begin with presenting the mean velocity profile in dimensional form measured at the exit for all three contractions. This has been done to examine how the mean flow velocity behaves with the radial distance along the contraction exit plane. In this way, the experimental data were provided, showing the uniformity of the measured velocity data, and therefore to perform a satisfactory comparison among all three contractions. Fig. 15 shows the mean velocity profiles measured at the exit plane of the 5th polynomial contraction for two various Reynolds numbers, $Re_c = 10^4$ and $Re_c = 33 \times 10^3$, utilizing the LDA in wall-normal (y) and spanwise (z) directions. A uniform velocity profiles could be clearly observed within the major part of the core region of the flow with velocity deviation ($\Delta U/U_\infty$) estimated to be less than $\pm 1\%$.

Fig. 16 is an illustration for the mean velocity profiles at the exit plane of the two-cubic arcs contraction measured in two directions, i.e. z and y, utilizing the LDA. The Reynolds numbers were $5.5 \times 10^3$ and $9.3 \times 10^3$ based on the bulk air velocity at the contraction exit and the contraction exit diameter. One might observe from the figure plausible agreement between profiles measured in $y$ and $z$ directions, assuring flow symmetry with deviation ($\Delta U/U_\infty$) estimated to be less than $\pm 1\%$. On the other hand, in Fig. 17 the mean velocity profile measured at the exit plane of the Witoszynski 2nd order polynomial contraction shows 4% lower velocity at the centerline when compared to velocity measured in wall proximity. This came in good agreement with the numerical prediction presented earlier in Fig. 13c.

Fig. 18 compares velocity profiles in dimensionless form for all contractions, i.e. the 5th order polynomial, the two-cubic arcs and the Witoszynski 2nd order polynomial contractions, under investigation. Good agreement is to be observed along the core region among all three contractions; however disagreement at the contraction wall layer is pronounced. The disagreement in the wall proximity is to be attributed to the abrupt change in the wall shape of the Witoszynski 2nd order polynomial contraction that resulted in rapid change in pressure gradient along the contraction wall as can be seen in Fig. 2, and numerically predicted in Figs. 10 and 11.

## 4. Conclusions and final remarks

Numerical and experimental data were presented and discussed in the various sections clarifying flow characteristics between inlet and exit planes of three wind tunnel contractions, resulting in the following conclusions:

1. The mean velocity profiles obtained from both the fifth order polynomial and the two-cubic arcs look similar in major parts of both contractions. The mean velocity profiles predicted for all contraction turned out to be in good agreement with the experimental results using the LDA.
2. The similar character of the turbulence intensity ($u'/U$) measured at the centerline of the exit plane for all three contractions under investigation indicates an independence of the exit centerline turbulence level on the contraction wall shape. Hence, if the contraction is mainly to be utilized for calibrating non-direct measuring techniques such as the hot wire anemometer, the core region of all three contraction tested is of equal interest.
3. The experimental and the numerical data showed that both the 5th order polynomial and the two cubic arcs contractions perform satisfactorily when compared with Witoszynski 2nd order polynomial contraction.
4. The overshoot observed in either the 5th order polynomial or the two cubic arcs contractions lies within the tolerance level, i.e. $\leqslant 10\%$, in wind tunnel applications as indicated by Morel [5].

5. Overall, the fifth-order polynomial contraction showed good exit flow characteristics with flow non-uniformity less than 0.5% when compared with the other two contractions, and therefore was regarded as the best of the three contractions, and was adopted for the large pipe facility (CoLa-Pipe) at LAS BTU-Cottbus-Sefftenberg.

Further experimental and numerical investigation is to be carried out with an added circular duct, having a short length, i.e. $\approx D_{outlet}$, to the contraction exit.

## Acknowledgement

The author acknowledges support received from LAS BTU-Cottbus-Senftenberg to carry out the experimental work utilizing its aeroacoutic facility. Appreciation, in particular, is to be expressed to Prof. Dr.-Ing. Christoph Egbers for his continuous support as well as to Prof. Dr.-Ing. Ennes Sarradj.

## References

[1] K. Saha, S. Som, M. Battistoni, Y. Li, S. Quan, P.K. Senecal, Numerical simulation of internal and near-nozzle flow of a gasoline direct injection fuel injector, J. Phys: Conf. Ser. 656/012100 (2015) 1–5.
[2] C.A. Zehrung, Comparative analysis of a low-speed wind tunnel designed for renewable energy applications (Master Theses), Purdue University, College of Technology, 2011.
[3] A. Abdelhamed, Y.-S. Yassen, M. ElSakka, Design optimization of three dimensional geometry of wind tunnel contraction, Ain Shams Eng. J. 6 (2015) 281–288.
[4] C. Witoszynski, Votraege aus dem gebiet der hydro- und aerodynamik, aus Stroemungstechnisches Messwesen bei S.G. Popow, VEB Verlag Technik Berlin, 1960 (Berlin 1924), pp. 32–36.
[5] T. Morel, Comprehensive design of axisymmetric wind tunnel contractions, ASME J. Fluids Eng. 225 (June) (1975) 225–233.
[6] T. Morel, Design of two-dimensional wind tunnel contractions, ASME J. Fluids Eng. No. 76- WA/FE-4 (December 1976) 1–7.
[7] A.K.M.F. Hussain, V. Ramjee, Effects of the axisymmetric contraction shape on incompressible turbulent flow, ASME J. Fluids Eng. 98 (Series I) (1976) 58.
[8] E.G. Tulapurkara, V.V.K. Bhalla, Experimental investigation of morel's method for wind tunnel contractions, ASME J. Fluids Eng. 110/45 (1–12) (1988) 45–47, March.
[9] J. Callan, I. Marusic, The effect of a changing aspect ratio through a wind tunnel contraction, AIAA- Denver, CO 19 (AIAA 2000-2461) (9-12 June 2000) 1–12.
[10] F.M. Fang, J.C. Chen, Y.T. Hong, Experimental and analytical evaluation of flow in a square-to-square wind tunnel contraction, J. Wind Eng. Ind. Aerodyn. 89 (2001) 247–262.
[11] a. G.W.J.E. Sargison, R. Rossi, Design and calibration of a wind tunnel with a two dimensional contraction, in: 15th Australasian Fluid Mechanics Conference, The University of Sydney, Sydney, Australia 5, 13–17 December 2004, pp. 1–4.
[12] M.J. Martin, K. Scavazze, I. Boyd, L. Bernal, Design of a low-turbulence, low-pressure wind-tunnel for micro-aerodynamics, J. Fluids Eng 128 (1045) (2006) 1–8. ASME SEPTEMBER.
[13] a.M.M.M.M. Dehghan, M. Soltani, K. Ghorbanian, Control of pressure gradient in the contraction of a wind tunnel, World Acad. Sci. Eng. Technol. 2 (4) (2008) 441–446.
[14] S. Guptaa, V. Dwivedib, J. Chauhanc, R. Goswamic, Design and simulation of open circuit blowdown type wind tunnel, in: International Congress on Computational Mechanics and Simulation (ICCMS), IIT Hyderabad, 10–12 December, 2012, pp. 1–12.
[15] P. Bradshaw, R.C. Paukhurt, The design of low-speed wind tunnels, Prog. Aeronautical Sci. (1964) 1.
[16] J.H. Bell, R.D. Mehta, Boundary layer predictions for small low speed contractions, AIAA J. 27 (3) (1988) 372–374.
[17] H. Tsien, On the design of the contraction cone for awwind wunnel, J. Aeronaut. Sci. 10 (2) (1943) 68–70, February.
[18] R. Smith, C. Wang, Contracting cones giving uniform throat speeds, J. Aeronaut. Sci. 11 (4) (1944) 356–360, October.
[19] S.M. Batill, M. Caylor, J. Hoffman, An experimental and analytic study of the flow in subsonic wind tunnel inlets, Air Force Wright Aeronaut. Lab. TR.-83-3109 (October) (1983) 58.
[20] S. Lain, J. Harjumaki, A theoretical study of axisymmetric contractions for lowspeed wind tunnels, Helsinki University of Technology, Laboratory of Aerodynamics, Report No. 75-A2, 1975.
[21] E.-S. Zanoun, M. Kito, C. Egbers, A study on flow transition and development in circular and rectangular ducts, ASME J. Fluids Eng. 131 (May) (2009) 1–11.
[22] B. Szczeniowski, Contraction cone for a wind tunnel, J. Aeronaut. Sci. 10 (8) (1943) 311, October.
[23] B. Thwaites, On the design of contractions for wind tunnels, Aeronautical Research Council Reports and Memorandum, 2278, 1946.
[24] N.T. Bloomer, Notes on the mathematical design of nozzles and wind tunnel contractions, J. Aeronaut. 8 (1957) 279–290.
[25] M.J. Cohen, N.J.B. Ritchie, Low-speed three-dimensional contraction design, J. Roy. Aeronaut. Soc. 66 (1962) 231.
[26] J.M. Floryan, W.S. Saric, Stability of gortler vorticies in boundary layers, J. AIAA 20 (3) (1982) 316–324.